Unusual suppression of a spin resonance mode by magnetic field in underdoped $NaFe_{1-x}Co_xAs$: Evidence for orbital-selective pairing

Yu Song,[1,2,*] Guotai Tan,[3] Chenglin Zhang,[1] Rasmus Toft-Petersen,[4] Rong Yu,[5] and Pengcheng Dai[1,3,†]

[1]Department of Physics and Astronomy, Rice University, Houston, Texas 77005, USA
[2]Department of Physics, University of California, Berkeley, California 94720, USA
[3]Center for Advanced Quantum Studies and Department of Physics, Beijing Normal University, Beijing 100875, China
[4]Helmholtz-Zentrum Berlin für Materialen und Energie, Hahn-Meitner-Platz 1, D-14109 Berlin, Germany
[5]Department of Physics and Beijing Key Laboratory of Opto-electronic Functional Materials and Micro-nano Devices, Renmin University of China, Beijing 100872, China

(Received 2 May 2018; revised manuscript received 13 July 2018; published 13 August 2018)

We use inelastic neutron scattering to study the fate of the two spin resonance modes in underdoped superconducting $NaFe_{1-x}Co_xAs$ ($x = 0.0175$) under applied magnetic fields. While an in-plane magnetic field of $B = 12$ T only modestly suppresses superconductivity and enhances static antiferromagnetic order, the two spin resonance modes display disparate responses. The spin resonance mode at higher energy is mildly suppressed, consistent with the field effect in other unconventional superconductors. The spin resonance mode at lower energy, on the other hand, is almost completely suppressed. Such dramatically different responses to applied magnetic field indicate distinct origins of the two spin resonance modes, resulting from the strongly orbital-selective nature of spin excitations and Cooper pairing in iron-based superconductors.

DOI: 10.1103/PhysRevB.98.064507

I. INTRODUCTION

Iron-based superconductivity appears in proximity to antiferromagnetic (AF) order [1–3], with spin fluctuations central to its pairing mechanism [1]. Like other families of unconventional superconductors [4,5], an intense spin resonance mode (SRM) is observed by inelastic neutron scattering in the superconducting state of iron-based superconductors [6], indicative of sign-reversed superconducting order parameters on different parts of the Fermi surface [7]. The SRM is believed to be an electron-hole spin-triplet bound state inside the superconducting gap [8,9], and its intensity acts as a proxy for superconducting pairing correlations [10]. Under in-plane magnetic fields well below the upper critical field, intensity of the SRM is observed to be only mildly suppressed [10–14], consistent with the notion that intensity of the SRM tracks the superconducting order parameter.

The electronic structure of iron-based superconductors is dominated by Fe $3d$ t_{2g} orbitals near the Fermi level, with hole-like Fermi surfaces at the zone center Γ and electron-like Fermi surfaces at the zone corner M, and the superconducting order parameter changes sign between these quasinested Fermi surfaces [7,15]. The presence of multiple Fe $3d$ orbitals near the Fermi level adds an orbital degree of freedom to the physics of iron-based superconductors, resulting in varying orbital characters on different parts of the Fermi surfaces [Fig. 1(a)] [16] and orbital-dependent strengths of electronic correlations [17,18]. Such strong orbital dependence then leads to orbital-selective Mott phases [19,20] and orbital-selective Cooper pairing [21,22] in iron-based superconductors.

The orbital degree of freedom also manifests in spin excitations, as exemplified by orbital-selective spin excitations in $LiFe_{1-x}Co_xAs$ [23] and double SRMs observed in underdoped $NaFe_{1-x}Co_xAs$ [24]. The double SRMs in underdoped $NaFe_{1-x}Co_xAs$ are suggested to result from orbital-dependent pairing, with superconducting gaps along the electron-like Fermi surface associated with different orbitals exhibiting differing superconducting gaps [Fig. 1(b)], and thus SRMs associated with different orbitals also appear at different energies. Double SRMs with different spin space anisotropy are also observed in optimally electron- [25], hole- [26], and isovalent-doped $BaFe_2As_2$ [27], although the two SRMs in these materials are not well separated in energy and are only revealed through neutron polarization analysis. In addition to orbital-selective pairing, the two modes have also been suggested to arise from the presence of static or slowly fluctuating magnetic order [28,29] or due to spin-orbit coupling (SOC) [30] that lifts spin-space degeneracy of the SRM [31–33]. Underdoped superconducting $NaFe_{1-x}Co_xAs$ offers a unique opportunity to probe the nature of its double SRMs using an applied magnetic field for several reasons. First, it exhibits competing superconductivity and AF order that can be tuned by a field accessible in a neutron scattering experiment. Second, the double SRMs are well separated in energy and can be resolved without polarization analysis. Finally, angle-resolved photoemission spectroscopy (ARPES) measurements revealed nodeless but anisotropic superconducting gaps at zero field [34], which may arise from orbital-selective pairing.

In this paper, we present an inelastic neutron scattering study of magnetic order and excitations in underdoped $NaFe_{1-x}Co_xAs$ ($x = 0.0175$) [24] under an in-plane magnetic

*yusong@berkeley.edu
†pdai@rice.edu

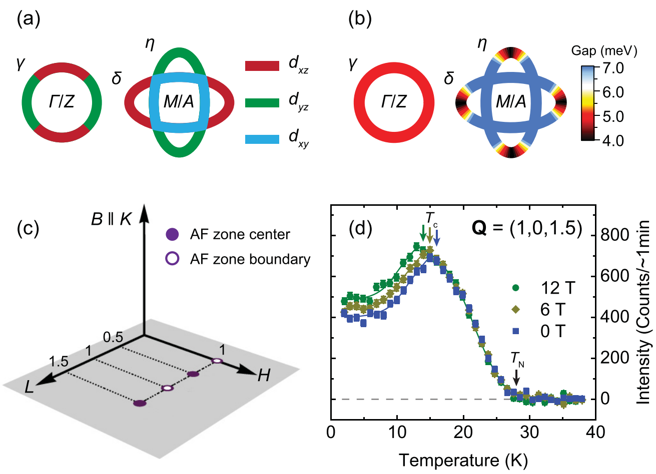

FIG. 1. (a) Schematic Fermi surface of underdoped $NaFe_{1-x}Co_xAs$, with dominant orbital contributions marked by different colors, based on ARPES measurements [49,50]. (b) Schematic of momentum-dependent superconducting gaps in underdoped $NaFe_{1-x}Co_xAs$, adapted from previous work [34]. The in-plane zone center is Γ or Z depending on k_z, and the in-plane zone corner is M or A depending on k_z. (c) Schematic of the $[H, 0, L]$ scattering plane. The magnetic field B is along K, perpendicular to the scattering plane. (d) Magnetic field dependence of the magnetic order parameter measured at $\mathbf{Q} = (1, 0, 0.5)$. A constant background has been subtracted. The solid lines are guides to the eye.

field. We find with a field of $B = 12$ T, superconductivity is modestly suppressed while AF order becomes slightly enhanced. Of the two SRMs in underdoped $NaFe_{1-x}Co_xAs$ [24], the mode at higher energy is modestly suppressed, in line with the similar modest suppression of superconductivity; the SRM at lower energy, however, is strongly suppressed and becomes indiscernible for $B \gtrsim 10$ T. The complete suppression of a SRM under magnetic field while superconductivity persists is highly unusual and could result from strongly orbital-selective pairing in iron pnictide superconductors. Our observations suggest superconducting gaps associated with orbitals that exhibit weak pairing strengths can be suppressed by magnetic fields well below the upper critical field, while bulk superconductivity persists due to orbitals that exhibit stronger pairing. Our work provides strong evidence for orbital-selective pairing and spin excitations in iron-based superconductors.

II. RESULTS

Single crystals of $NaFe_{1-x}Co_xAs$ ($x = 0.0175$) were grown using the self-flux method and have been previously studied using transport [35], ARPES [34], and neutron scattering measurements [35–37] at zero field. Inelastic neutron scattering experiments were carried out using the FLEXX three-axis spectrometer at Helmholtz-Zentrum Berlin, Germany. Fixed $k_f = 1.55$ Å^{-1} was used for all the measurements, and higher-order neutrons are eliminated by using a velocity selector before the monochromator and a Be filter after the sample. We denote momentum transfer $\mathbf{Q} = (Q_x, Q_y, Q_z)$ in reduced lattice unit (r.l.u.) as $\mathbf{Q} = (H, K, L)$, with $H = \frac{aQ_x}{2\pi}$, $K = \frac{bQ_y}{2\pi}$, and $L = \frac{cQ_z}{2\pi}$, using $a \approx b \approx 5.57$ Å and $c \approx 6.97$ Å appropriate for the orthorhombic magnetically ordered phase of $NaFe_{1-x}Co_xAs$ [35,38]. In this notation, magnetic Bragg peaks appear at $\mathbf{Q} = (1, 0, L)$ with $L = 0.5, 1.5, 2.5\ldots$, whereas integer L values correspond to AF zone boundaries along the c axis [Fig. 1(c)]. Our samples were aligned in the $[H, 0, L]$ scattering plane and placed inside a magnet with the field direction perpendicular to the scattering plane along K [Fig. 1(c)].

$NaFe_{1-x}Co_xAs$ ($x = 0.0175$) exhibits competing superconductivity and AF order with an ordered moment $\sim 0.03\ \mu_B$/Fe [35]. Magnetic field dependence of the AF order parameter is shown in Fig. 1(d) for $B = 0$, 6, and 12 T. AF order onsets below $T_N \approx 28$ K regardless of field, and the intensity above T_c is unaffected by applied field. This indicates that unlike in-plane uniaxial pressure [39–42], for $T > T_c$ an applied magnetic field up to $B = 12$ T affects neither the AF ordered moment size nor population of the AF domains that order at $\mathbf{Q}_1 = (1, 0)$ or $\mathbf{Q}_2 = (0, 1)$ in underdoped $NaFe_{1-x}Co_xAs$. The AF order parameters are reduced with the onset of superconductivity below T_c, indicative of the competing nature of the two orders in iron pnictides [43,44]. With applied field, T_c is reduced from its zero-field value $T_c \approx 16$ K to $T_c \approx 14$ K for $B = 12$ T. The modest suppression of T_c is consistent with the large upper critical field $B_{c2} \gtrsim 40$ T in underdoped $NaFe_{1-x}Co_xAs$ [45]. Due to the suppression of superconductivity under applied field, the AF order parameter inside the superconducting state becomes enhanced with applied field. At $T = 2$ K, the magnetic intensity becomes $\sim 20\%$ stronger for $B = 12$ T compared to $B = 0$ T. Overall, the effects of a $B = 12$ T in-plane magnetic field on $NaFe_{1-x}Co_xAs$ ($x = 0.0175$) appear modest; it reduces T_c by $\sim 10\%$ while enhancing the AF ordered moment also by $\sim 10\%$.

Magnetic field dependence of spin fluctuations at $\mathbf{Q} = (1, 0, 0.5)$ is shown in background-subtracted constant-$\mathbf{Q}$ scans in Fig. 2(a) (see Appendix for details on background subtraction). We find the normal state response above T_c to be field independent, similar to other iron-based superconductors [46], and therefore the normal state data collected at different fields are combined (see Appendix for field dependence of normal state excitations). Below T_c for $B = 0$ T, we observe SRMs centered at $E_{r1} \approx 3.25$ meV and $E_{r2} \approx 6.5$ meV, with a valley at $E \approx 4.5$ meV that display little or no enhancement below T_c, in agreement with previous work [24]. Surprisingly, at $B = 12$ T the mode at E_{r1} becomes strongly suppressed, while the mode at E_{r2} is only mildly suppressed, resulting in a single discernible SRM at $B = 12$ T.

To verify the dramatically different fate of the SRMs under $B = 12$ T, temperature dependence of the two modes are compared at $B = 0$ T and $B = 12$ T in Figs. 2(b) and 2(d). While both SRMs at E_{r1} and E_{r2} display clear anomalies at T_c under both $B = 0$ T and $B = 12$ T, the SRM at E_{r1} becomes much weaker under $B = 12$ T [Fig. 2(b)] while the mode at E_{r2} is hardly affected [Fig. 2(d)]. Similar behavior is also seen at the AF zone boundary along the c axis at $\mathbf{Q} = (1, 0, 1)$ [Fig. 2(c)], where it is possible to cover the full energy range of the SRM at E_{r2}. Since the SRM at E_{r2} is L independent [24], the modest suppression seen in the energy range $5 \leqslant E \leqslant 10$ meV at $\mathbf{Q} = (1, 0, 1)$ also applies to $\mathbf{Q} = (1, 0, 0.5)$. On the other hand, the SRM at E_{r1} displays significant L dependence and

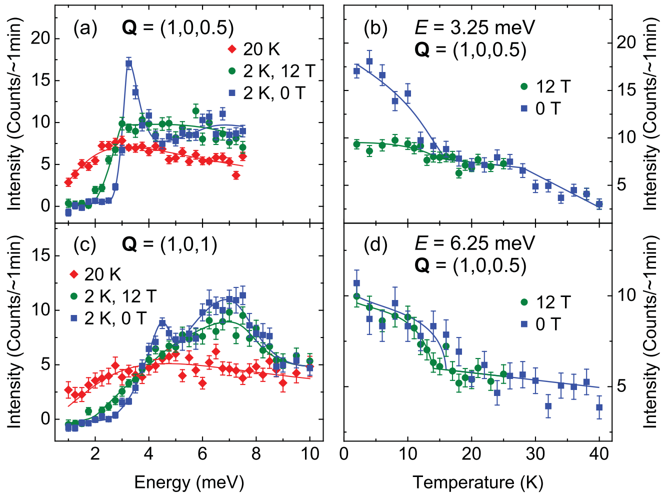

FIG. 2. (a) Background-subtracted constant-**Q** scans at $\mathbf{Q} = (1, 0, 0.5)$. (b) Temperature dependence at $\mathbf{Q} = (1, 0, 0.5)$ and $E = 3.25$ meV under $B = 0$ T and 12 T, with background subtracted. (c) Background-subtracted constant-**Q** scans at $\mathbf{Q} = (1, 0, 1)$. (d) Temperature dependence at $\mathbf{Q} = (1, 0, 0.5)$ and $E = 6.25$ meV under $B = 0$ T and 12 T, with background subtracted. The solid lines are guides to the eye. See Appendix for details on background subtraction.

is much weaker at $\mathbf{Q} = (1, 0, 1)$ [24], nevertheless it is also strongly suppressed at $B = 12$ T, similar to the behavior at $\mathbf{Q} = (1, 0, 0.5)$ in Fig. 2(a).

Having shown that the SRM at E_{r2} is only modestly suppressed at $B = 12$ T, similar to the behavior of SRMs under applied magnetic field in other unconventional superconductors [10–14], we focus on the SRM at E_{r1} which responds much more dramatically to applied field and study its evolution as a function of applied field. We mapped out the intensity of $T = 2$ K magnetic excitations at $\mathbf{Q} = (1, 0, 0.5)$ as a function of energy (2 meV $\leqslant E \leqslant$ 4.5 meV) and field (0 T $\leqslant B \leqslant$ 14 T), as shown in Fig. 3(a). Strong suppression of the SRM at E_{r1} with applied field is immediately apparent. Notably despite the strong suppression in intensity, we do not observe softening for energy of the mode up to $B \approx 8$ T, and at higher fields the mode is no longer discernible.

To see how the applied magnetic field affects the SRM at different energies, we show detailed scans from Fig. 3(a) at representative energies in Figs. 3(b)–3(e), compared to the 20 K response (horizontal lines, since the 20 K response is field independent). At $E = 2.5$ meV [Fig. 3(b)], which is inside a superconductivity-induced spin gap at zero field, magnetic intensity gradually increases with increasing field. This indicates the superconductivity-induced spin gap becomes smaller with applied field [Fig. 3(a)] and is similar to previous observations in optimal-doped $BaFe_{1.9}Ni_{0.1}As_2$ [13]. At $E = E_{r1} = 3.25$ meV [Fig. 3(c)], intensity is quickly suppressed with applied field and plateaus for $B \gtrsim 8$ T, despite superconductivity persisting to $B \gtrsim 40$ T [45]. This behavior is completely different from what was previously seen in $BaFe_{1.9}Ni_{0.1}As_2$ [13], where suppression of the SRM tracks suppression of superconductivity under applied magnetic field [13]. At $E = 3.75$ meV [Fig. 3(d)], corresponding to a shoulder of the SRM at E_{r1}, while the intensity shows

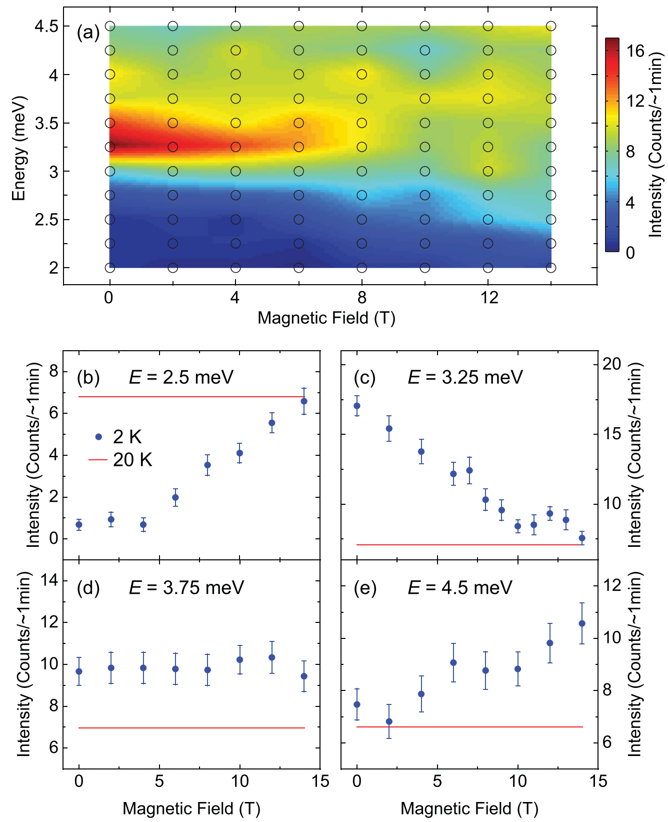

FIG. 3. (a) Color-coded and interpolated magnetic field dependence of low-energy magnetic fluctuations at $\mathbf{Q} = (1, 0, 0.5)$ and $T = 2$ K, with background subtracted. The circles correspond to points where measurements were taken. Magnetic field dependence of magnetic fluctuations at $\mathbf{Q} = (1, 0, 0.5)$ and $T = 2$ K for (b) $E = 2.5$ meV, (c) $E = 3.25$ meV, (d) $E = 3.75$ meV, and (e) $E = 4.5$ meV. The flat red lines are from fits at 20 K shown in Fig. 2(a), which do not show magnetic field dependence. See Appendix for details on background subtraction.

clear enhancement relative to the normal state, no significant field dependence is observed. At $E = 4.5$ meV [Fig. 3(e)], corresponding to the valley between the two SRMs, the intensity gradually increases with applied field, confirming the valley between E_{r1} and E_{r2} disappears with increasing field [see also Fig. 2(a)].

Further insight into how the low-energy spin dynamics evolve under applied magnetic field can be gained by examining constant-energy scans shown in Fig. 4. At $E = E_{r1} = 3.25$ meV, scans along $(H, 0, 0.5)$ [Fig. 4(a)] and $(1, 0, L)$ [Fig. 4(b)] both confirm the strong suppression of the SRM at $E = E_{r1}$ under $B = 12$ T. Moreover, correlation length along L for the response at $B = 12$ T is significantly shorter compared to $B = 0$ T, suggesting the intense SRM at zero field involving spins in many Fe-As layers is fully suppressed, replaced by fluctuations of the spins that display weak correlations between Fe-As planes. Suppression of the superconductivity-induced spin gap can be clearly seen in Fig. 4(c) at $E = 2.5$ meV, while at zero field there is almost no magnetic signal, a clear peak is observed under $B = 12$ T. At $E = 4.5$ meV [Fig. 4(d)], which corresponds to E_{r1} at integer L values, and which at $L = 0.5$ corresponds to the

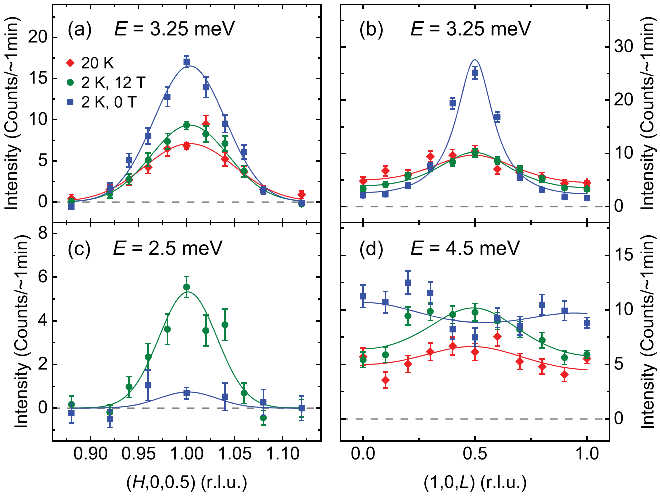

FIG. 4. (a) Background-subtracted constant-energy scans along $(H, 0, 0.5)$ for $E = 3.25$ meV, (b) along $(1, 0, L)$ for $E = 3.25$ meV, (c) along $(H, 0, 0.5)$ for $E = 2.5$ meV, and (d) along $(1, 0, L)$ for $E = 4.5$ meV. Solid lines in (a) and (c) are fits to Gaussian peaks, and solid lines in (b) and (d) are fits to lattice Lorentzian peaks. See Appendix for details on background subtraction.

valley between E_{r1} and E_{r2}, display dramatically different L dependence between $B = 0$ T and $B = 12$ T. At zero field, we find the magnetic fluctuations to be peaked at integer L values, consistent with a previous report [24]. However, under $B = 12$ T the magnetic fluctuations peak at $L = 0.5$, similar to the normal state response. This dramatic change in L dependence also evidences the SRM at E_{r1}, which disperses along L from $E_{r1} = 3.25$ meV at $L = 0.5$ to $E_{r1} = 4.5$ meV at $L = 1$, is fully suppressed under $B = 12$ T, replaced by magnetic fluctuations that are always centered at $L = 0.5$.

III. DISCUSSION

Our results show that the low-energy SRM is strongly suppressed by a magnetic field well below B_{c2}, while the high-energy mode is only weakly suppressed. The complete suppression of the low-energy SRM when static magnetic order is gradually enhanced with field [Fig. 1(a)] suggests that it is not directly associated with AF order. Given T_c is only weakly modified by a magnetic field much smaller than B_{c2}, the suppression of the low-energy SRM is also unlikely to be due to reduction of the dominant superconducting gaps that determine T_c.

On the other hand, the low-energy SRM is spin anisotropic while the high-energy one is spin isotropic [47]. Such a spin-space anisotropy reflects different orbital characters associated with the two resonances, after taking into account the effect of spin-orbit coupling. In fact, theoretical calculation [48] has found that the high-energy SRM is mainly associated with the d_{xy} orbital, and the low-energy one involves d_{xz} and d_{yz} orbitals. The orbital character of the Fermi surface in $NaFe_{1-x}Co_xAs$ [Fig. 1(a)] [49,50] and the anisotropic superconducting gaps [Fig. 1(b)] [34] suggest that the d_{xy} orbital exhibits stronger superconducting pairing whereas d_{xz}/d_{yz} has weaker pairing strength, in contrast to FeSe with pairing mainly due to d_{xz}/d_{yz} orbitals [22]. Within a five-orbital

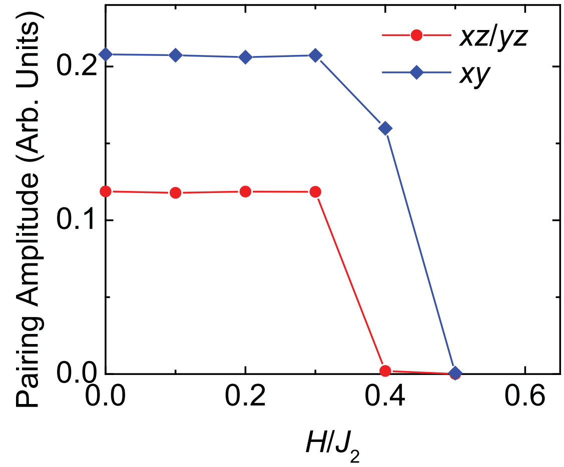

FIG. 5. Orbital-selective destruction of the superconducting pairing amplitudes by the applied magnetic field in a five-orbital t-J model. Shown are the leading pairing channels with $s\pm$ symmetry in xz/yz and xy orbitals. The horizontal axis is the ratio of applied magnetic field H and the next-nearest-neighbor exchange coupling J_2.

t-J model [48], we studied how the superconducting pairing evolves under a magnetic field. Our main result is summarized in Fig. 5. The pairing strengths of the leading $s\pm$ pairing channels in both the xz/yz and xy orbitals are stable against weak fields but are reduced when the field becomes strong. Interestingly, the suppression of the pairing amplitudes undergoes in an orbital-selective way. At an intermediate field, the small superconducting gaps associated with d_{xz}/d_{yz} orbitals become strongly suppressed by the applied magnetic field, while T_c is determined by superconducting gaps associated with d_{xy} orbitals, which remain robust for a similar field. The disparate fate of the two SRMs in underdoped $NaFe_{1-x}Co_xAs$ under applied field then results from their orbital-selective nature, with the high-energy mode associated with d_{xy} orbitals and maintains its intensity, while the low-energy mode involves d_{xz}/d_{yz} orbitals and is strongly suppressed.

Finally, we note that suppression of the low-energy SRM by a field well below B_{c2} in underdoped $NaFe_{1-x}Co_xAs$ is reminiscent of amplitude Higgs mode's behavior under magnetic field in superconducting 2H-$NbSe_2$ [51–53], which also display strong suppression by a magnetic field well below B_{c2} while exhibiting little or no softening of energy of the mode. The field sensitivity of the Higgs mode in 2H-$NbSe_2$ is suggested to arise from suppression of the superconducting volume due to the formation of vortices [53], which cannot account for what we observe in underdoped $NaFe_{1-x}Co_xAs$. This is because intensity of the SRM at E_{r2}, which is reflective of the superconducting volume, is only weakly affected by the magnetic field.

ACKNOWLEDGMENTS

We thank Manh Duc Le and Diana Lucía Quintero-Castro for assistance in preliminary neutron scattering measurements, and Ming Yi and Dung-Hai Lee for helpful discussions. The neutron-scattering work at Rice University is supported by the United States DOE, BES DE-SC0012311 (P.D.). A part of the materials work at Rice is supported by the Robert A.

Welch Foundation through Grant No. C-1839 (P.D.). We thank HZB for the allocation of neutron radiation beam time.

APPENDIX

1. Background subtraction

Background for constant-**Q** scans should be measured at positions with the same |**Q**| but no magnetic signal. From constant-energy scans shown in Fig. 4 and in previous work [24], magnetic excitations in underdoped $NaFe_{1-x}Co_xAs$ are relatively sharp along H and broad along L, we have therefore chosen $\mathbf{Q} = (0.8, 0, L)$ to measure the background. Constant-**Q** scans before background subtraction are shown in Fig. 6(a) for $\mathbf{Q} = (1, 0.5)$ and in Fig. 6(c) for $\mathbf{Q} = (1, 0, 1)$, together with respective background measurements at $\mathbf{Q} = (0.8, 0, 0.902)$ and $\mathbf{Q} = (0.8, 0, 1.25)$. The background is then fit to an empirical form and the fit values have been subtracted from results presented in Figs. 2 and 3.

Raw data of constant-energy scans were fit with a Gaussian or a lattice Lorentzian peak plus a linear background; the linear background was constrained to be identical for different temperatures and applied fields. The resulting linear background was subtracted from the raw data, with the results shown in Fig. 4.

2. Field dependence of normal state excitations

Figures 6(b) and 6(d), respectively, show constant-**Q** scans at 20 K for $\mathbf{Q} = (1, 0, 0.5)$ and $\mathbf{Q} = (1, 0, 1)$, under different applied fields. Similar to previous results on $BaFe_{2-x}Ni_xAs_2$ [46], we do not observe significant field dependence for the normal state excitations, therefore we combined our data measured at 20 K under different fields.

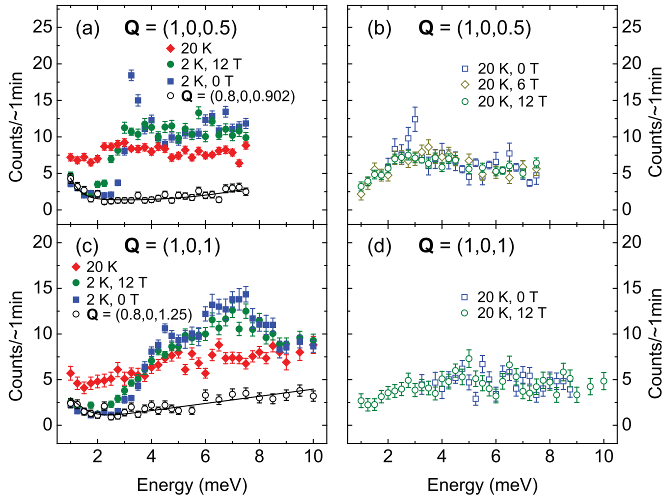

FIG. 6. (a) Constant-**Q** scans at $\mathbf{Q} = (1, 0, 0.5)$, without background subtraction. Background measured at $\mathbf{Q} = (0.8, 0, 0.902)$ is shown for comparison, and the solid line is an empirical fit to the background. (b) Background-subtracted constant-**Q** scans at $\mathbf{Q} = (1, 0, 0.5)$ for $T = 20$ K under different applied fields. (c) Constant-**Q** scans at $\mathbf{Q} = (1, 0, 1)$, without background subtraction. Background measured at $\mathbf{Q} = (0.8, 0, 1.25)$ is shown for comparison, and the solid line is an empirical fit to the background. (d) Background-subtracted constant-**Q** scans at $\mathbf{Q} = (1, 0, 1)$ for $T = 20$ K under different applied fields.

[1] D. J. Scalapino, Rev. Mod. Phys. **84**, 1383 (2012).
[2] P. Dai, Rev. Mod. Phys. **87**, 855 (2015).
[3] D. S. Inosov, C. R. Phys. **17**, 60 (2016).
[4] J. Rossat-Mignod, L. P. Regnault, C. Vettier, P. Bourges, P. Burlet, J. Bossy, J. Y. Henry, and G. Lapertot, Physica C **185**, 86 (1991).
[5] C. Stock, C. Broholm, J. Hudis, H. J. Kang, and C. Petrovic, Phys. Rev. Lett. **100**, 087001 (2008).
[6] A. D. Christianson, E. A. Goremychkin, R. Osborn, S. Rosenkranz, M. D. Lumsden, C. D. Malliakas, I. S. Todorov, H. Claus, D. Y. Chung, M. G. Kanatzidis, R. I. Bewley, and T. Guidi, Nature (London) **456**, 930 (2008).
[7] P. J. Hirschfeld, M. M. Korshunov, and I. I. Mazin, Rep. Prog. Phys. **74**, 124508 (2011).
[8] M. Eschrig, Adv. Phys. **55**, 47 (2006).
[9] Y. Sidis, S. Pailhès, V. Hinkov, B. Fauqué, C. Ulrich, L. Capogna, A. Ivanov, L.-P. Regnault, B. Keimer, and P. Bourges, C. R. Phys. **8**, 745 (2007).
[10] P. Dai, H. A. Mook, G. Aeppli, S. M. Hayden, and F. Doğan, Nature (London) **406**, 965 (2000).
[11] P. Bourges, H. Casalta, L. P. Regnault, J. Bossy, P. Burlet, C. Vettier, E. Beaugnon, P. Gautier-Picard, and R. Tournier, Physica B **234–236**, 830 (1997).
[12] J. Wen, G. Xu, Z. Xu, Z. W. Lin, Q. Li, Y. Chen, S. Chi, G. Gu, and J. M. Tranquada, Phys. Rev. B **81**, 100513(R) (2010).
[13] J. Zhao, L.-P. Regnault, C. Zhang, M. Wang, Z. Li, F. Zhou, Z. Zhao, C. Fang, J. Hu, and P. Dai, Phys. Rev. B **81**, 180505 (2010).
[14] S. Li, X. Lu, M. Wang, H.-q. Luo, M. Wang, C. Zhang, E. Faulhaber, L.-P. Regnault, D. Singh, and P. Dai, Phys. Rev. B **84**, 024518 (2011).
[15] G. R. Stewart, Rev. Mod. Phys. **83**, 1589 (2011).
[16] M. Yi, Y. Zhang, Z.-X. Shen, and D. Lu, npj Quantum Mater. **2**, 57 (2017).
[17] Z. P. Yin, K. Haule, and G. Kotliar, Nat. Mater. **10**, 932 (2011).
[18] Luca de' Medici, G. Giovannetti, and M. Capone, Phys. Rev. Lett. **112**, 177001 (2014).
[19] M. Yi, D. H. Lu, R. Yu, S. C. Riggs, J.-H. Chu, B. Lv, Z. K. Liu, M. Lu, Y.-T. Cui, M. Hashimoto, S.-K. Mo, Z. Hussain, C. W. Chu, I. R. Fisher, Q. Si, and Z.-X. Shen, Phys. Rev. Lett. **110**, 067003 (2013).
[20] R. Yu and Q. Si, Phys. Rev. Lett. **110**, 146402 (2013).
[21] E. M. Nica, R. Yu, and Q. Si, npj Quantum Mater. **2**, 24 (2017).
[22] P. O. Sprau, A. Kostin, A. Kreisel, A. E. Böhmer, V. Taufour, P. C. Canfield, S. Mukherjee, P. J. Hirschfeld, B. M. Andersen, and J. C. Séamus Davis, Science **357**, 75 (2017).
[23] Y. Li, Z. Yin, X. Wang, D. W. Tam, D. L. Abernathy, A. Podlesnyak, C. Zhang, M. Wang, L. Xing, C. Jin, K. Haule, G. Kotliar, T. A. Maier, and P. Dai, Phys. Rev. Lett. **116**, 247001 (2016).

[24] C. Zhang, R. Yu, Y. Su, Y. Song, M. Wang, G. Tan, T. Egami, J. A. Fernandez-Baca, E. Faulhaber, Q. Si, and P. Dai, Phys. Rev. Lett. **111**, 207002 (2013).

[25] P. Steffens, C. H. Lee, N. Qureshi, K. Kihou, A. Iyo, H. Eisaki, and M. Braden, Phys. Rev. Lett. **110**, 137001 (2013).

[26] C. Zhang, M. Liu, Y. Su, L.-P. Regnault, M. Wang, G. Tan, Th. Brückel, T. Egami, and P. Dai, Phys. Rev. B **87**, 081101 (2013).

[27] D. Hu, W. Zhang, Y. Wei, B. Roessli, M. Skoulatos, L. Pierre Regnault, G. Chen, Y. Song, H. Luo, S. Li, and P. Dai, Phys. Rev. B **96**, 180503 (2017).

[28] W. Lv, A. Moreo, and E. Dagotto, Phys. Rev. B **89**, 104510 (2014).

[29] M. Wang, M. Yi, H. L. Sun, P. Valdivia, M. G. Kim, Z. J. Xu, T. Berlijn, A. D. Christianson, S. Chi, M. Hashimoto, D. H. Lu, X. D. Li, E. Bourret-Courchesne, P. Dai, D. H. Lee, T. A. Maier, and R. J. Birgeneau, Phys. Rev. B **93**, 205149 (2016).

[30] S. V. Borisenko, D. V. Evtushinsky, Z.-H. Liu, I. Morozov, R. Kappenberger, S. Wurmehl, B. Büchner, A. N. Yaresko, T. K. Kim, M. Hoesch, T. Wolf, and N. D. Zhigadlo, Nat. Phys. **12**, 311 (2016).

[31] Y. Song, H. Man, R. Zhang, X. Lu, C. Zhang, M. Wang, G. Tan, L.-P. Regnault, Y. Su, J. Kang, R. M. Fernandes, and P. Dai, Phys. Rev. B **94**, 214516 (2016).

[32] M. M. Korshunov, Y. N. Togushova, I. Eremin, and P. J. Hirschfeld, J. Supercond. Nov. Magn. **26**, 2873 (2013).

[33] D. D. Scherer and B. M. Andersen, Phys. Rev. Lett. **121**, 037205 (2018).

[34] Q. Q. Ge, Z. R. Ye, M. Xu, Y. Zhang, J. Jiang, B. P. Xie, Y. Song, C. L. Zhang, P. Dai, and D. L. Feng, Phys. Rev. X **3**, 011020 (2013).

[35] G. Tan, Y. Song, C. Zhang, L. Lin, Z. Xu, T. Hou, W. Tian, H. Cao, S. Li, S. Feng, and P. Dai, Phys. Rev. B **94**, 014509 (2016).

[36] S. V. Carr, C. Zhang, Y. Song, G. Tan, Y. Li, D. L. Abernathy, M. B. Stone, G. E. Granroth, T. G. Perring, and P. Dai, Phys. Rev. B **93**, 214506 (2016).

[37] C. Zhang, W. Lv, G. Tan, Y. Song, S. V. Carr, S. Chi, M. Matsuda, A. D. Christianson, J. A. Fernandez-Baca, L. W. Harriger, and P. Dai, Phys. Rev. B **93**, 174522 (2016).

[38] S. Li, C. de la Cruz, Q. Huang, G. F. Chen, T.-L. Xia, J. L. Luo, N. L. Wang, and P. Dai, Phys. Rev. B **80**, 020504 (2009).

[39] C. Dhital, Z. Yamani, W. Tian, J. Zeretsky, A. S. Sefat, Z. Wang, R. J. Birgeneau, and S. D. Wilson, Phys. Rev. Lett. **108**, 087001 (2012).

[40] Y. Song, S. V. Carr, X. Lu, C. Zhang, Z. C. Sims, N. F. Luttrell, S. Chi, Y. Zhao, J. W. Lynn, and P. Dai, Phys. Rev. B **87**, 184511 (2013).

[41] D. W. Tam, Y. Song, H. Man, S. C. Cheung, Z. Yin, X. Lu, W. Wang, B. A. Frandsen, L. Liu, Z. Gong, T. U. Ito, Y. Cai, M. N. Wilson, S. Guo, K. Koshiishi, W. Tian, B. Hitti, A. Ivanov, Y. Zhao, J. W. Lynn, G. M. Luke, T. Berlijn, T. A. Maier, Y. J. Uemura, and P. Dai, Phys. Rev. B **95**, 060505 (2017).

[42] W. Wang, J. T. Park, R. Yu, Y. Li, Y. Song, Z. Zhang, A. Ivanov, J. Kulda, and P. Dai, Phys. Rev. B **95**, 094519 (2017).

[43] A. D. Christianson, M. D. Lumsden, S. E. Nagler, G. J. MacDougall, M. A. McGuire, A. S. Sefat, R. Jin, B. C. Sales, and D. Mandrus, Phys. Rev. Lett. **103**, 087002 (2009).

[44] J. Larsen, B. M. Uranga, G. Stieper, S. L. Holm, C. Bernhard, T. Wolf, K. Lefmann, B. M. Andersen, and C. Niedermayer, Phys. Rev. B **91**, 024504 (2015).

[45] S. Ghannadzadeh, J. D. Wright, F. R. Foronda, S. J. Blundell, S. J. Clarke, and P. A. Goddard, Phys. Rev. B **89**, 054502 (2014).

[46] M. Wang, H. Luo, M. Wang, S. Chi, J. A. Rodriguez-Rivera, D. Singh, S. Chang, J. W. Lynn, and P. Dai, Phys. Rev. B **83**, 094516 (2011).

[47] C. Zhang, Y. Song, L.-P. Regnault, Y. Su, M. Enderle, J. Kulda, G. Tan, Z. C. Sims, T. Egami, Q. Si, and P. Dai, Phys. Rev. B **90**, 140502 (2014).

[48] R. Yu, J.-X. Zhu, and Q. Si, Phys. Rev. B **89**, 024509 (2014).

[49] Y. Zhang, C. He, Z. R. Ye, J. Jiang, F. Chen, M. Xu, Q. Q. Ge, B. P. Xie, J. Wei, M. Aeschlimann, X. Y. Cui, M. Shi, J. P. Hu, and D. L. Feng, Phys. Rev. B **85**, 085121 (2012).

[50] M. Yi, D. H. Lu, R. G. Moore, K. Kihou, C.-H. Lee, A. Iyo, H. Eisaki, T. Yoshida, A. Fujimori, and Z.-X. Shen, New J. Phys. **14**, 073019 (2012).

[51] R. Sooryakumar and M. V. Klein, Phys. Rev. Lett. **45**, 660 (1980).

[52] R. Sooryakumar and M. V. Klein, Phys. Rev. B **23**, 3213 (1981).

[53] P. B. Littlewood and C. M. Varma, Phys. Rev. B **26**, 4883 (1982).